金星夜側電離層で見られる
Ionospheric Tail Rays

下田 忠宏 (京大理・M1)

2002 年夏の学校

1 Introduction

金星には固有磁場がないため、金星電離圏起源粒子の惑星間空間への散逸は地球と異なった様相をみせる。これらの現象のうち、夜側電離圏では高ベータプラズマが夜側に引き延ばされた Tail Ray が見られる。Tail ray をはじめ、金星夜側電離層での現象について、その概念的な想像図を図 1 にしめす。

2 Observation of Ionospheric Tail Rays

PVO が夜側で periapsis となるような軌道を通ったときの、OETP(Orbiter electron temperature probe) による観測により、図 2 に示すデータが得られた [Brace et al., 1987]。高度 1000km 以上での電子密度観測では 2 つ以上の電子密度上昇が見られ、これらの山が、"tail rays" と呼ばれている。

2.1 Tail Rays の高度分布

各軌道について periapsis 高度別にデータを見てみると (図 2)、1150km ではっきりとした 2 本の tail rays が見られ (Orbit1187)、高度 1500km より上では (図 2 の右上)Tail rays は 3 本観測されている (Orbiter1639)。

また、これら 2 本、3 本の tail rays の出現緯度を見てみると、2 本の場合は赤道を挟んで南北に 1 本づつ tail ray が見られ、3 本の場合は赤道付近に 1 本、南北に 1 本ずつの tail ray が見られる。

2.2 Existence of O^+

OETP、OMAG、OIMS(O^+_{st})、および ONMS(O^+_f) での同時観測によって得られたデータを図 3 に示す。高エネルギー酸素イオン (O^+) は superthermal ion

よりも少量であるのだが、エネルギーは 40eV を越え、また、ONMS により、それらが tailward に流れていることがが確認された (図 4)。

2.3 磁場構造

図 3 の磁場データを見ると、tail ray で B_x が逆転していて、2 つの tail ray の間の trough では磁場の強さは tail ray よりも強い。これは、tail ray の両端で電流が流れていて、かつ、tail ray と trough の境界ではプラズマの静圧と磁気が釣り合いが保たれているということが予想できる。

また、tail ray が存在しているときの夜側電離層の磁場について各成分を見ると、x 成分が支配的で、磁力線が北半球で tailward、南半球で venusward であることがわかる。すなわち、電離層によって drape された磁力線をみているということになる。

3 A Model

以上に紹介された観測事実に対し、そのモデルが Luhmann,1991 によって提唱された。

ここでは、テスト粒子をいくつか走らせ、その動きを見ることで tail rays ができる様子を見ている。PVO による観測例 (図 5) をもとにした、電離層によって drape された磁力線のモデル、および、金星プラズマの flow の速度 (全て反太陽向き) モデル (図 6) を与え、テスト粒子 (O^+) を走らせた (この時の粒子の初期位置は terminator にしている)。これによって得られた、粒子の軌道、そして、粒子の相対的密度を (図 7,8) に示す。

これによると、tail rays らしき構造がみられ、また、これの focusing には重力も寄与していることが分かる。このことから、低エネルギーの O^+ イオンが convection 電場によって pick-up され、磁力線の draping によって粒子が focus されている、ということができる。

また、図 (8) に示されている密度構造を見ると、terminator 起源の粒子が楕円形、8 の字を経て、南北の 2 つに focus されていく様子が見て取れる。

ただし、このような tail ray の構造は高度だけでなくて IMF にも依存することに注意しなければならない。

4 References

- L. H. Brace, W. T. Kasprzak, H. A. Taylor, R. F. Theis, C. T. Russell, A. Barnes, J. D. Mihalov, and D. M. Hunten, The Ionotail of Venus: Its Configuraion and Evidence for Ion Escape, J. Geophys. Res., **92**, A1, 15-26, 1987

図7

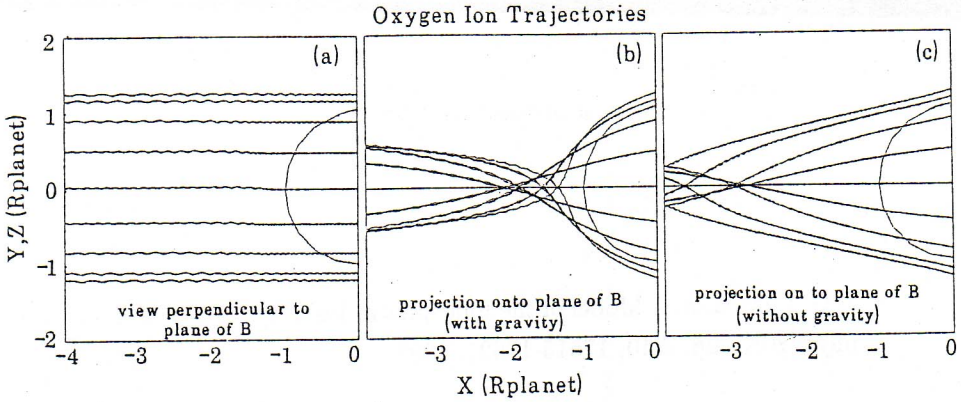

Fig. 3. Sample O^+ ion trajectories in the wake field model of Figure 2 from a source region located around the terminator at 1000km altitude. (*a*) Meridian plane projection (viewed along the interplanetary field direction); (*b*) projection in the plane containing the magnetic field; (*c*) same as Figure 3*b* but without gravity.

図8

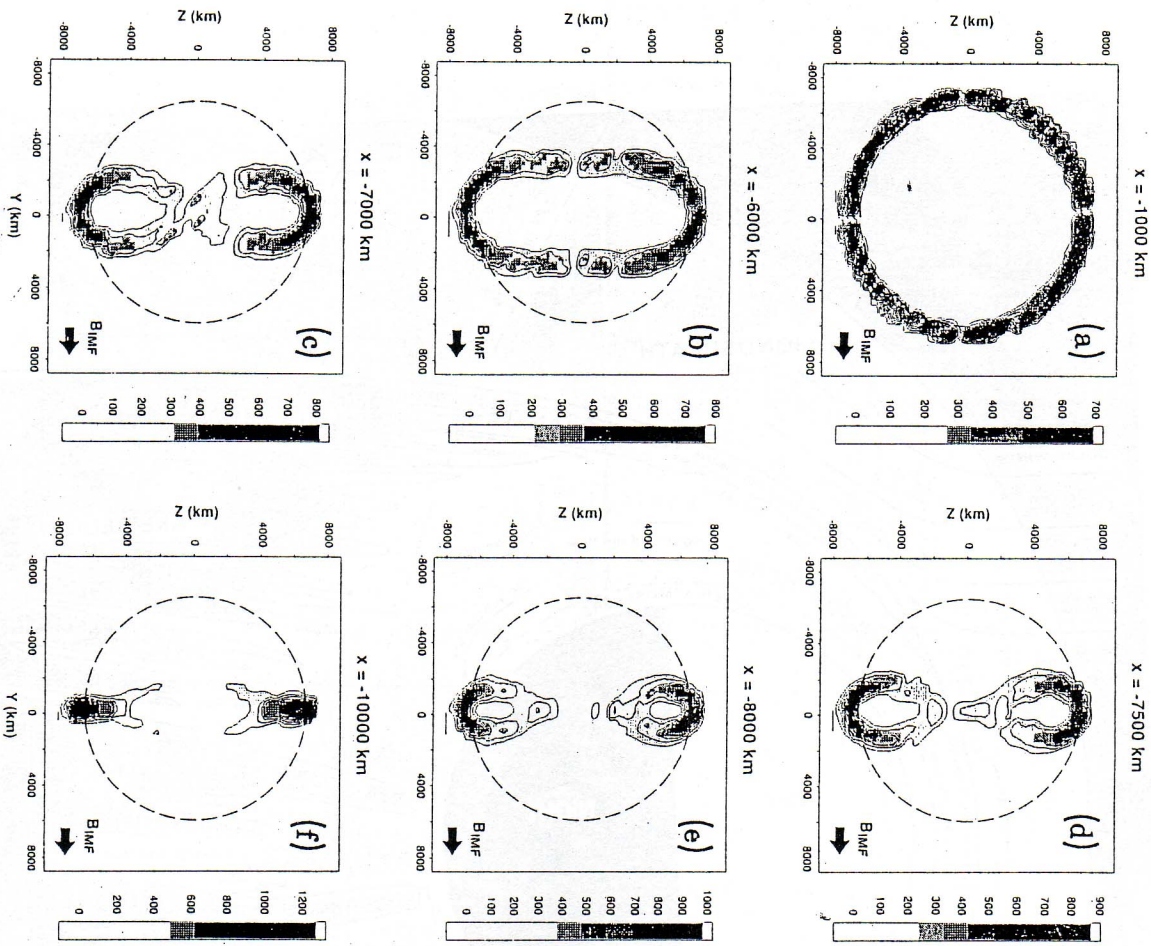

Fig. 4. Cross sections of relative "density" contours through the model low-energy ion tail at various down-tail distances (x). Notice that the number of tail rays observed depends on both the altitude of the spacecraft and the angle between its trajectory and the interplanetary field B_{IMF}. The dashed circles indicate optical shadow boundary locations.

図9

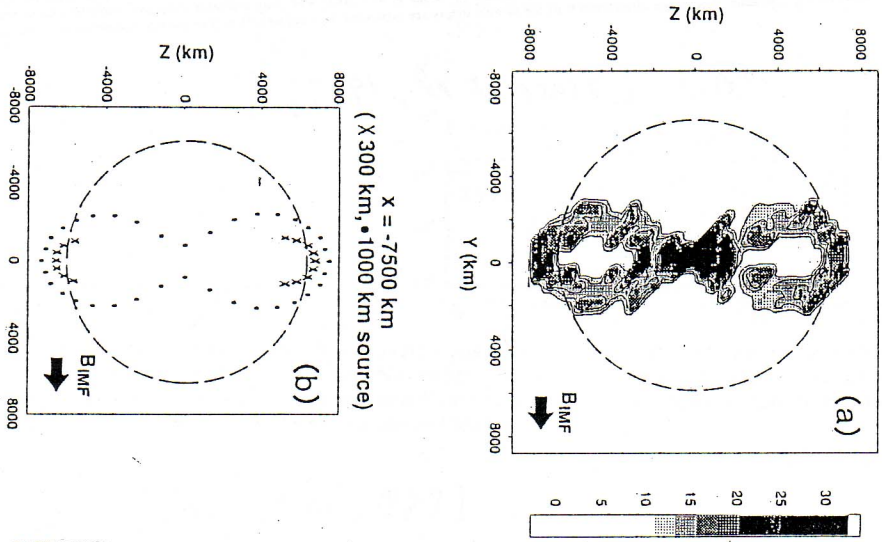

Fig. 5. (*a*) Version of the x = -7500 km panel from Figure 4 showing the average ion energies at each position in the structure. (*b*) Ion trajectory intersections originating from low (300 km) and high (1000 km) altitudes, showing that the particles in the central part of the figure eight structure come from the higher terminator altitudes, where the motional electric field in the model is stronger.

図7a ... [Lühmann, 1993]

- J. G. Luhmann, A Model of the Ionospheric Tail Rays of Venus, J. Geophys. Res., **98**, A10, 17615-17621, 1993

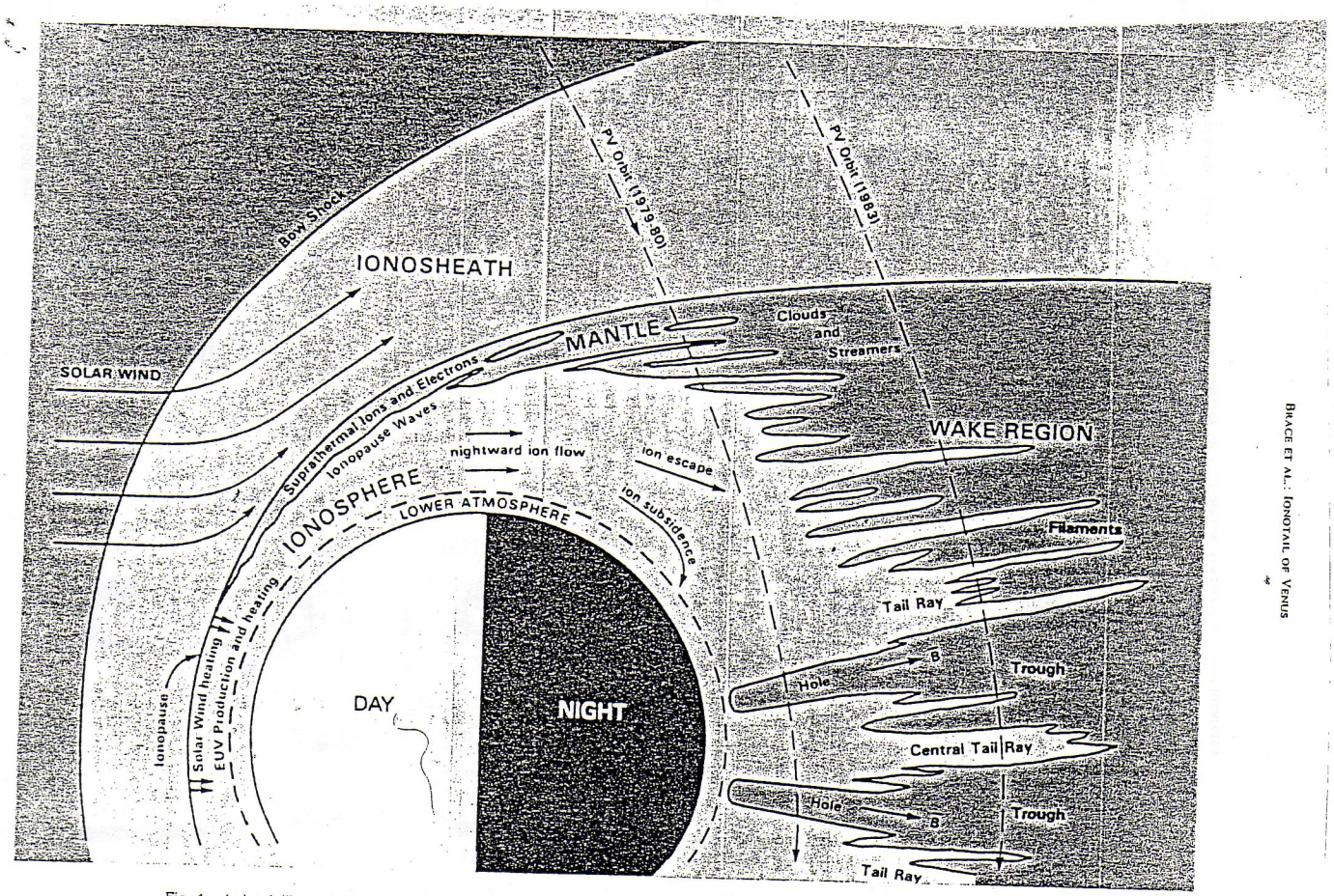

Fig. 4. A sketch illustrating the typical structure of the Venus ionotail based on hundreds of PVO crossings such as those shown in Figures 2 and 3. This drawing was adapted from an earlier sketch by *Brace et al.* [1983] who had available only low altitude measurements in the ionosphere. The scale of both the ionosphere and the sample orbits are expanded by a factor of 2 or 3 relative to the planet to allow annotation.

図 1 [Brace et al., 1987]

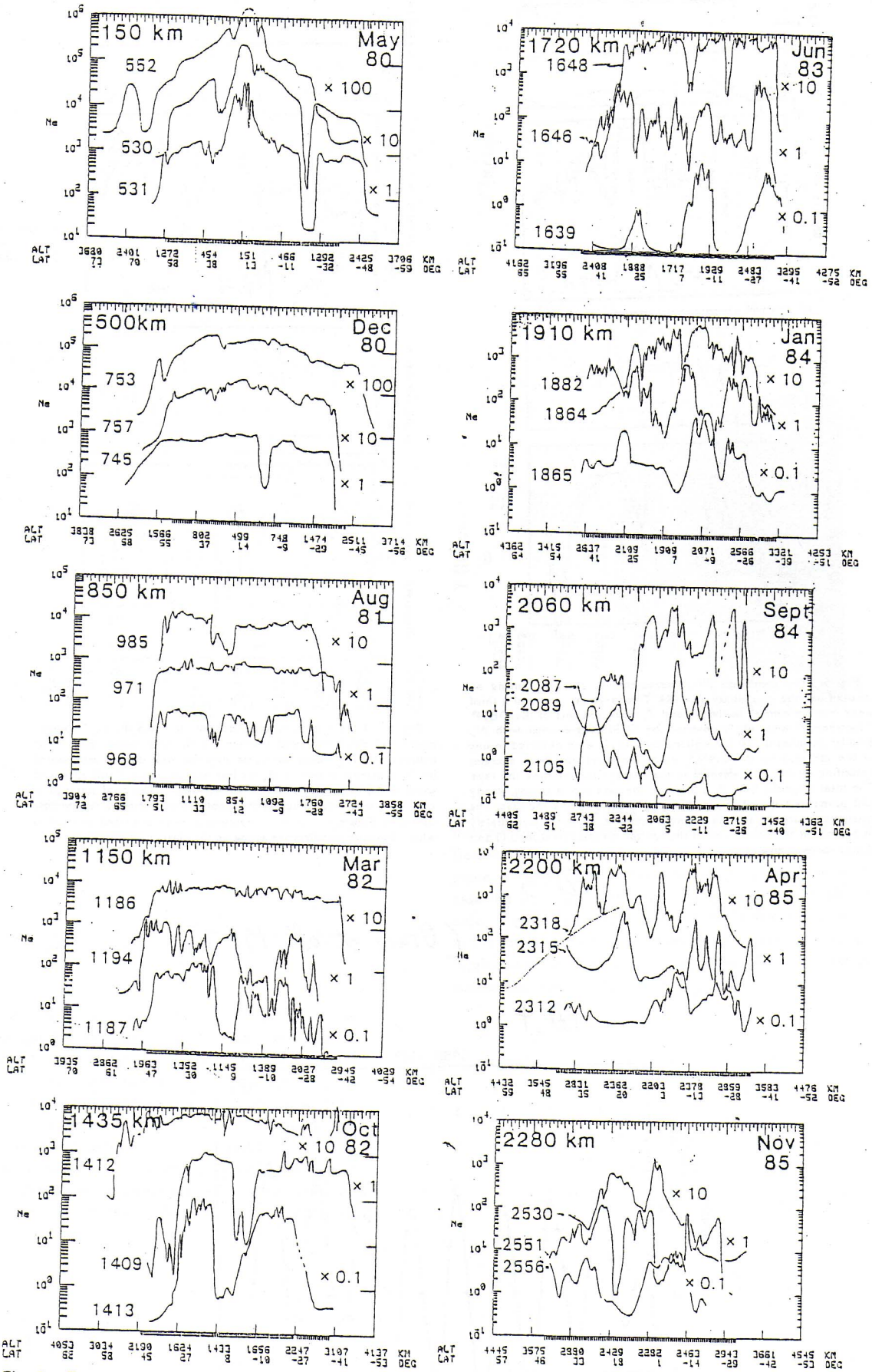

Fig. 2. Groups of three typical N_e profiles selected from ionotail passages of PVO at successively higher altitudes (periapsis altitude listed at upper left) between May 1980 and November 1985. Orbit numbers are listed at the left and multiplying factors at the right used to reduce overlap. Tail rays and filamentary structure have become more evident since early 1982 when PVO crossings of the umbra (vertical bars) rose above 1000 km.

図 2 [Brace et al., 1987]

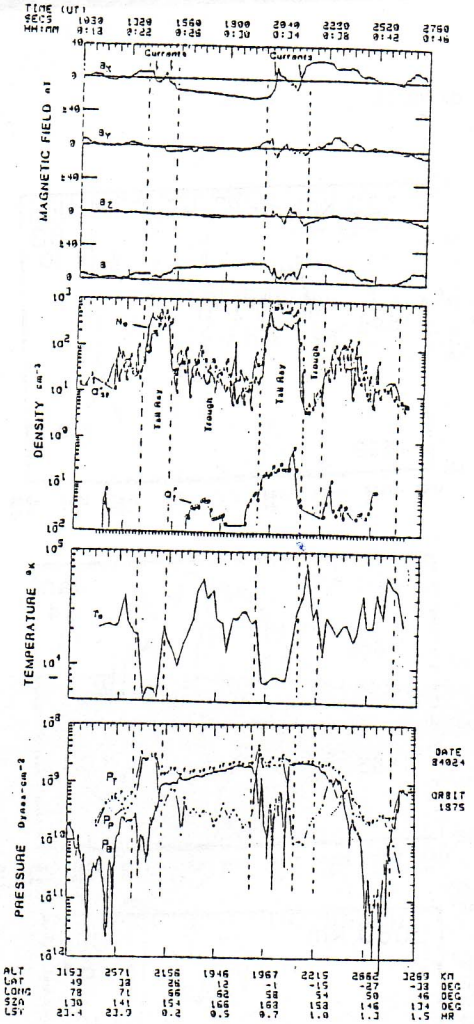

Fig. 5. The combined PVO measurements obtained during an ionotail passage on January 24, 1984. Two large tail rays and a third weak one are evident in the N_e and T_e measurements of the OETP. Superthermal ions, O_{st}^+, observed by OIMS, agree well with N_e. Smaller densities of fast ionospheric ions, O_f^+, were observed in one of the tail rays by the ONMS which measures ions with energies exceeding 40 eV. T_e is elevated in the troughs surrounding the rays. The total magnetic field, B, is lower in the rays and is strong, steady and primarily tailward, B_x, in the troughs surrounding the rays. The plasma pressure, P_p, and the magnetic pressure, P_B, are approximately in balance at the boundaries of the central ray (00.32–00.36 UT) and strong currents flow there.

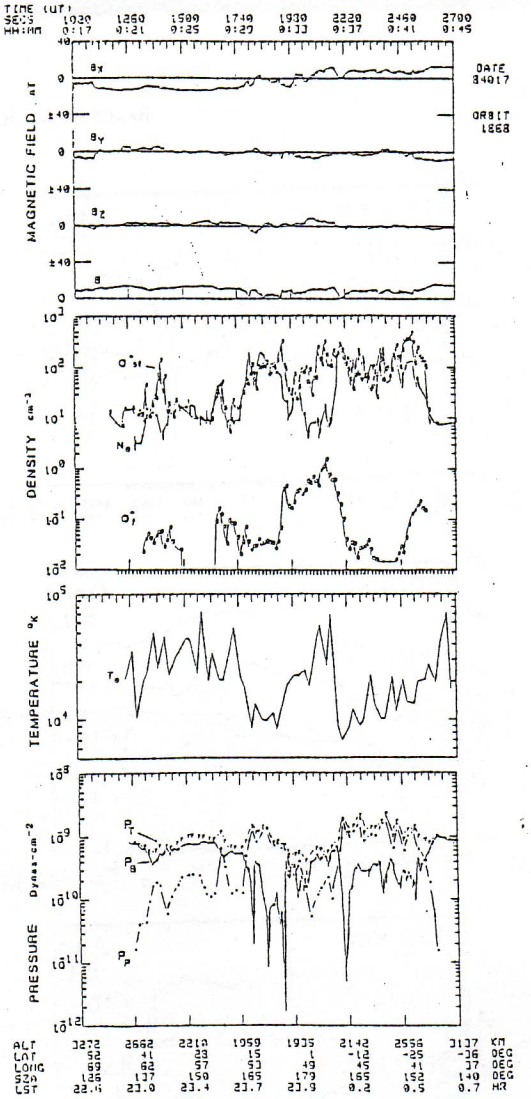

Fig. 6. A less typical ionotail crossing in which the O_f^+ component (>40 eV) is enhanced between the tail rays, rather than in the troughs, and O_{st}^+ does not agree with the total density represented by N_e. Currents evident in B_x are less well defined but still appear at some of the tail ray boundaries defined by N_e. The total static pressure P_T is less uniform across the ionotail than the more typical case shown in Figure 5. This may represent a more disturbed ionotail in which dynamic pressures are acting on the plasma.

図 3

[Brace et al., 1987]

図 4

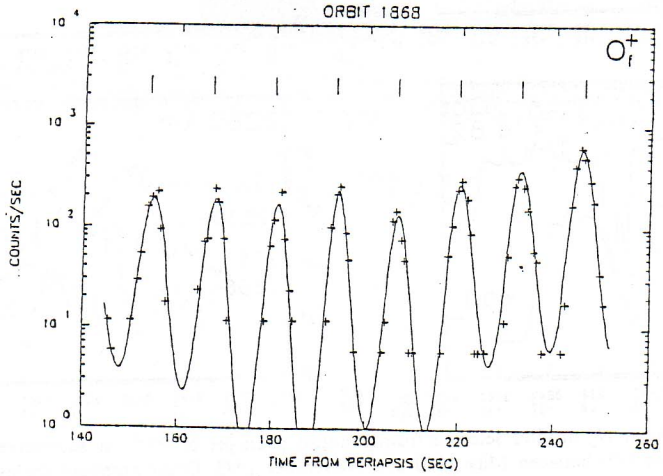

Fig. 7. Spin modulated ONMS signal for O_f^+ (>40 eV) obtained while crossing the fast oxygen ion enhancement within the trough between 0033–0037 UT on orbit 1868 (Figure 6). The solid curve represents a sinusoidal fit to the measurements (pluses). The O_f^+ flux peaks within a few degrees of the solar direction (vertical tick marks), thus showing that the ion flow is tailward. Similar outward flows are seen on most other ionotail passages that have been analyzed in this fashion.

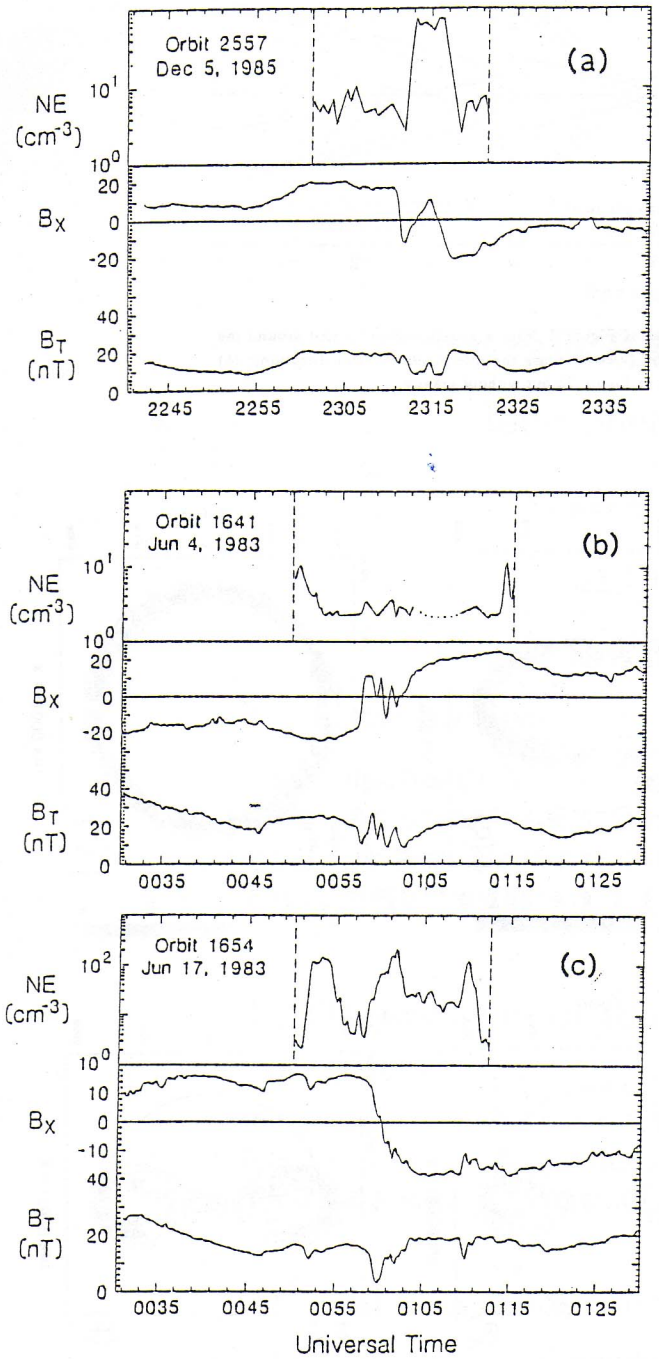

Fig. 1. Time series of Pioneer Venus Orbiter Langmuir probe (upper panels) and magnetometer (lower panels) data from *Dubinin et al.* [1991], showing characteristic one (*a*), two (*b*), and three (*c*) tail ray electron density structures and tail lobe-like magnetic field structure observed in the Venus near-wake at altitudes of ~1500-2300 km. The B_x component of the field is in the sun-Venus direction. B_T is the field magnitude. The vertical dashed lines in the electron density (NE) panels mark the times of crossing the optical shadow boundaries. (Photoelectron backgrounds occur outside of these boundaries, making the measurements of low densities uncertain.)

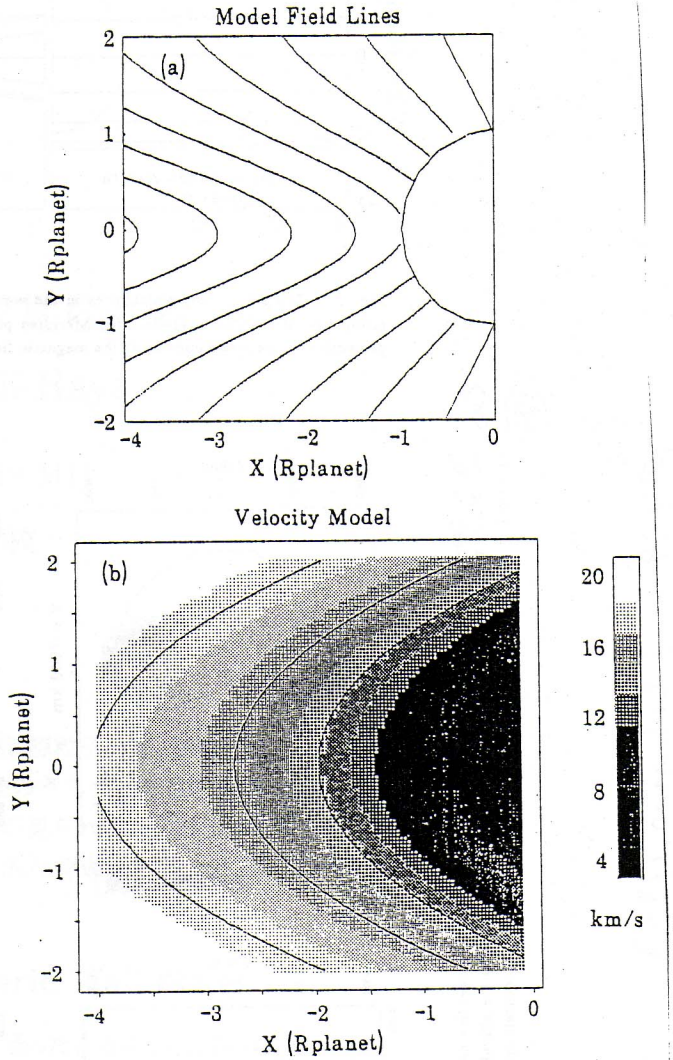

Fig. 2. (*a*) Magnetic field lines in the plane containing the interplanetary magnetic field and the x (sun-Venus) axis for the wake field model used here. (*b*) Model flow velocity contours for the same plane as Figure 2*a* except that the outline of Venus is left out. In this case the structure is cylindrically symmetric with respect to the x axis. For both panels, the assumption is that the model applies only in the low-altitude wake and not in the magnetosheath proper or at large down-tail distances, where the flow is expected to substantially accelerate. (Note: For Venus, $R_{planet} \approx 6350$ km.)

図5

図6

[Luhmann, 1993]

図7

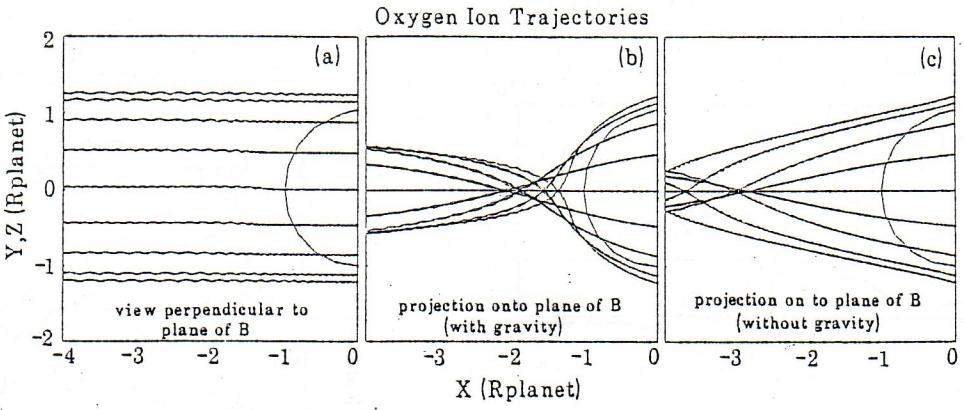

Fig. 3. Sample O^+ ion trajectories in the wake field model of Figure 2 from a source region located around the terminator at 1000km altitude. (*a*) Meridian plane projection (viewed along the interplanetary field direction); (*b*) projection in the plane containing the magnetic field; (*c*) same as Figure 3*b* but without gravity.

図8

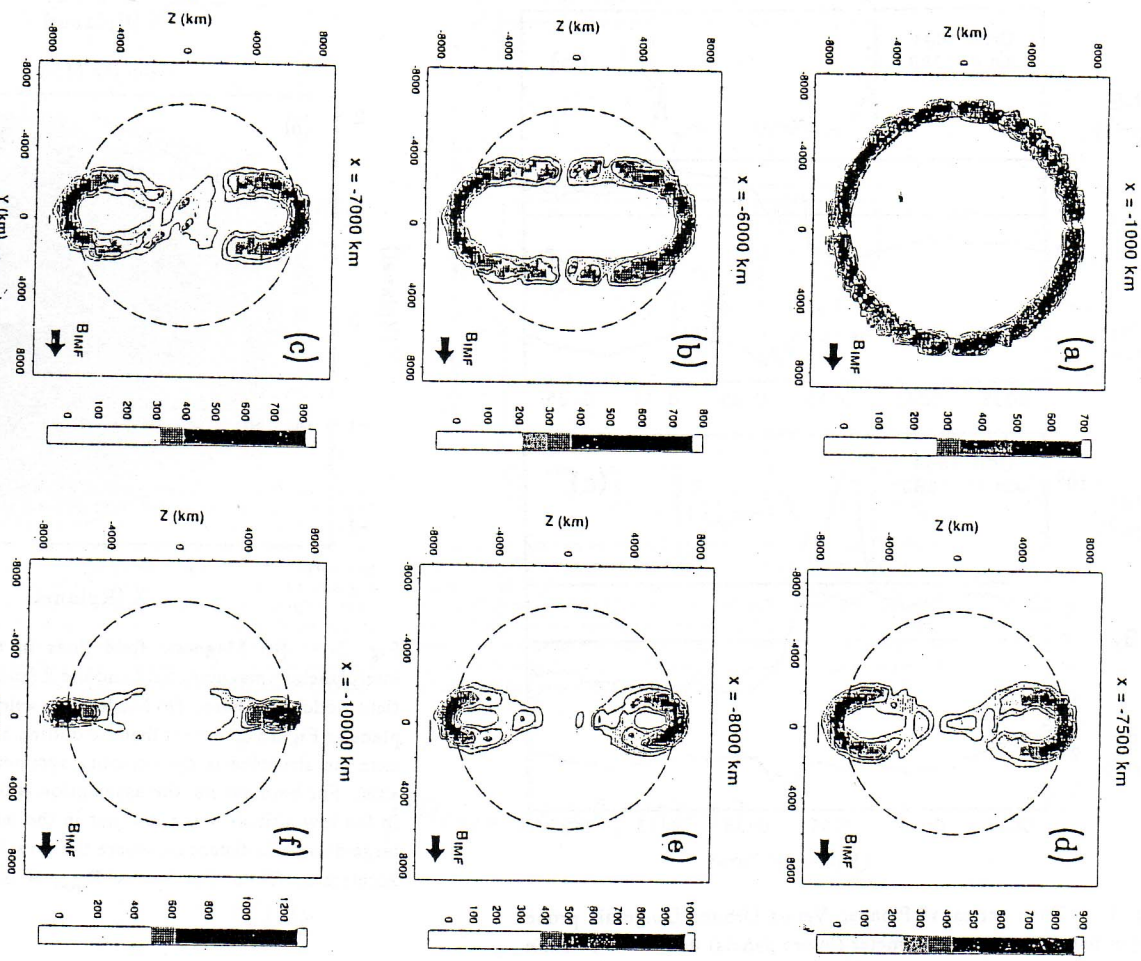

Fig. 4. Cross sections of relative "density" contours through the model low-energy ion tail at various down-tail distances (x). Notice that the number of tail rays observed depends on both the altitude of the spacecraft and the angle between its trajectory and the interplanetary field B_{IMF}. The dashed circles indicate optical shadow boundary locations.

図9

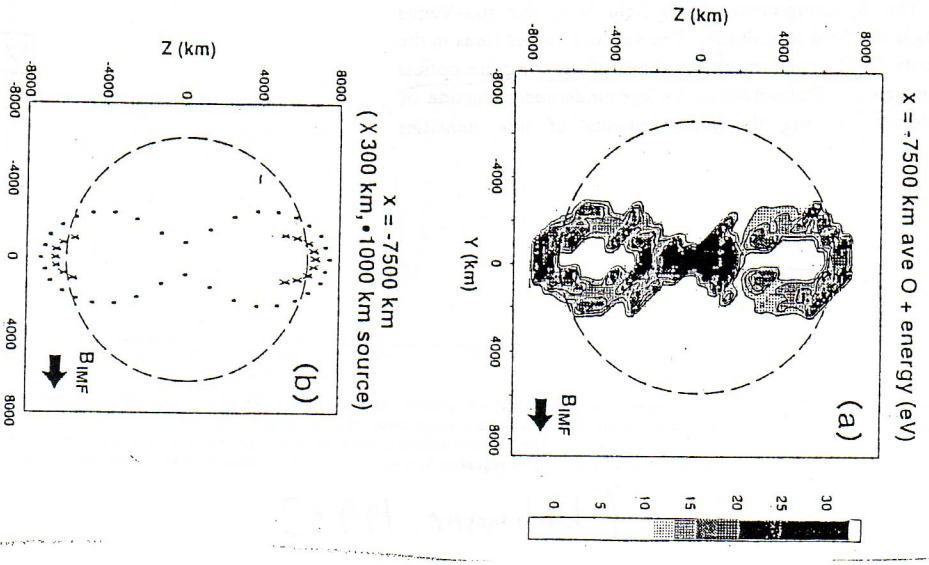

Fig. 5. (*a*) Version of the x = -7500 km panel from Figure 4 showing the average ion energies at each position in the structure. (*b*) Ion trajectory intersections originating from low (300 km) and high (1000 km) altitudes, showing that the particles in the central part of the figure eight structure come from the higher terminator altitudes, where the motional electric field in the model is stronger.

図7,9 … [Luhmann, 1993]